Self-sustaining power supplies for low-power electronics

Albert C. van der Woerd, Michel A. Bais, Leo P. de Jong, and Arthur H.M. van Roermund,
Delft University of Technology, Department of Electrical Engineering,
Electronic Research Laboratory
Mekelweg 4, 2628 CD Delft, The Netherlands

ABSTRACT

This paper describes three methods to provide self-sustaining micro-power supplies for low-power electronic systems. The primary energy sources are light, small temperature differences, and wasted electromagnetic energy, respectively. We start with the first method, i.e. a low-power photo-voltaic power converter from solar cells to a rechargeable battery. Its development is the furthest of the three methods, therefore it is the main contents of this paper. It will be used in a directional hearing aid. The converter has an efficiency that lies between 70% and 85%. The battery will be stuck onto the back of the power-converter chip. We also show a structured derivation of the necessary solar cell area. The possibilities of the use of small temperature differences will be demonstrated with a brief description of a voltage-to-voltage converter from a few millivolts to a few volts. Possible applications are self-sustaining power supplies for implanted medical devices such as pacemakers and neuro-stimulators. Investigations into the third method, i.e. the use of wasted electromagnetic energy, have recently started, and will only be touched lightly on.

1. INTRODUCTION

We start with the description of a self-sustaining power supply for a directional adapter for hearing aids. Research within the Department of Applied Physics of Delft University of Technology has made clear that the use of a directional microphone in a hearing aid can improve the intelligibility in group conversation. A result of improvement in intelligibility will be the disappearance of the puzzled look on the faces of the hard of hearing in a crowded room.
A directional microphone is made by use of a microphone array. Because of the distance between the individual microphones, there is a time delay between the audio signals received. The microphone array, completed with delay lines, yields a directional microphone. For a more detailed discussion the reader is referred to [1].

The acceptance of this hearing aid by consumers and producers is dependent on the volume, the ergonomics and the total appearance of the hearing aid. A prototype, comprising a pipe tied to a pair of glasses with a separate 9 V battery,

clearly showed that the total circuit must be integrated in low-power electronics. The aim of the current project is to house all electronics plus the microphones and the battery in a pair of spectacles, as depicted in Figure 1. An existing hearing aid, in the T position, will be used to amplify the received audio. The coupling between the pair of spectacles and the hearing aid will be by a magnetic transmitter situated in the wing behind the ear of the spectacles.

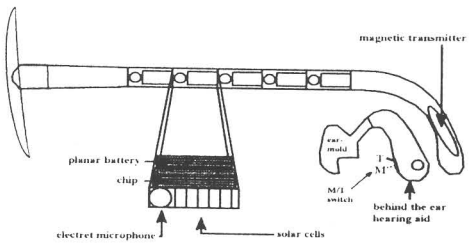

Fig 1, The directional hearing aid in a pair of spectacles.

Figure 1 shows that the hearing aid will be supplied with solar cells and an integrated rechargeable back-up battery. This implies that the directional hearing aid will be self-supporting.

Both the battery and the solar cells will be mounted together with the electronics on a very thin PCB and implemented in the wings of a pair of spectacles. A feasibility study[2] on the power management has made clear that 0.013 cm^3 in the wing will be used by the battery to provide 50 μAh. In Section 3 we show that $\approx$1 cm^2 of the total surface of the wing must be covered with solar cells to deliver 60 μW. The electronics will operate at a maximum of 1.2 V and the battery will be a Lithium-ion type with a solid electrolyte, to guarantee a minimum life time of 5 years.[3]

The power converter between the solar cells and the battery, together with the electronics, must be integrated on a chip and function under the changing output of the solar cell caused by changes in light intensity. After an investigation of literature it became clear that a switched-capacitor converter was the only converter that makes use of capacitors only. The capacitors are easy to make on chip, whereas this converter has a medium efficiency for low power applications.[4] The switched-capacitor converter can be adapted to the changing conditions of the solar cell by controlling its frequency.

It also became clear[5] that a power-converter system with efficiency η_a parallel to the switched-capacitor converter with medium efficiency η_b can improve the total effective power-system efficiency (η_e). Figure 2 shows the principle of parallel power conditioning.

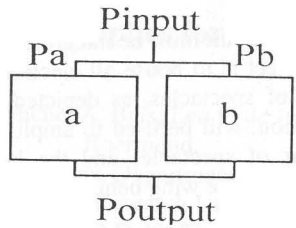

Fig.2, Parallel power conditioning.[4]

The input power is split into P_a and P_b, which are transferred with efficiencies η_a and η_b, respectively. The total effective power-system efficiency is described by:

$$\eta_e = \frac{\eta_a . P_a + \eta_b . P_b}{P_{input}} \quad (1)$$

Note that the effective efficiency only increases when η_a is higher than the efficiency η_b of the switched-capacitor converter. In [5] the use of a capacitor combined with a maximum power-point tracker is recommended to construct a parallel power converter. This capacitor represented by η_a is very efficient. It is not a direct power converter but an energy reservoir for the switched-capacitor converter. The capacitor, together with the switched-capacitor converter, is a parallel power converter, which can improve the total efficiency (η_e) by a maximum amount of 35%.

A description of the parallel power converter is given in Section 2. In Section 3, we discuss the derivation of the solar cell surface. In Section 4, we show a block diagram of the complete system. Section 5 is on the comparison of the requirements with the simulated results.

Section 6 contains a brief description of the use of small temperature differences as a power source for (implanted) medical devices. A converter from a few millivolts (the output voltage of a thermo-pile) to some volts, is shown. Finally, section 7 contains a brief discussion of the feasibility to use wasted electromagnetic waves as a power source for low-power electronics.

2. THE PARALLEL POWER CONVERTER

In this Section, we explain the implementation and the mathematics of the parallel power converter, described theoretically in the previous Section. Figure 3 shows the generic diagram of the total power converter with the capacitor C_a and the switched-capacitor converter on the left and right sides, respectively. The capacitor C_a must be minimally 10 times larger than the total capacity C_1 in order to perform as a parallel power converter. The number of capacitors C_1, to

be used depends on the voltage difference between battery and solar cell. The average output voltage of the solar cell is about 1.6 V, while the battery has a maximum charged voltage of 1.2 V.

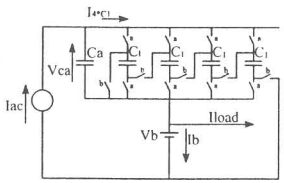

Fig.3, Total power converter.

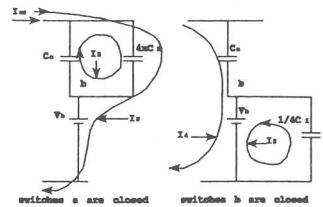

Fig.4, Currents through the converter.

When the switches 'a' are closed the minimum voltage difference V_{Ca} on the capacitors $C_a//n*C_1$ is 0.4 V. Closing the switches 'b' results in the series connection of the capacitors C_1 in parallel with the battery. Even in this case it is possible to transfer energy from the series connected capacitors to the load without discharging the battery. This can be done if the voltage ($n*V_{Ca}$) across the series connected capacitors C_1 is larger than the battery voltage V_b. This leads to the following boundary condition: $n*V_{Ca}>V_b$. Thus, n must be larger than 3. n in this setup equals 4, because of practical restrictions on the used switches.

In the last part of this Section, we explain how the power conversion takes place under the assumption that I_{load} is 0. The switches 'a' and b, in Figure 3, are controlled by two clocks ϕa and ϕb, which are in anti-phase. The switches 'a' are closed during T_a and the switches 'b' during T_b. During T_a, the capacitors C_1 are charged with current I_{4*C1} , as depicted in Figure 5.

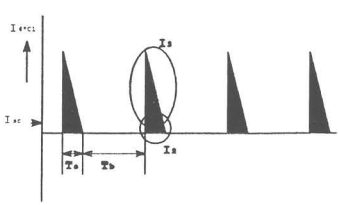

Fig. 5, Current I_{4*C1}

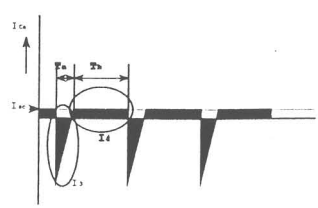

Fig. 6, Current I_{C4}

Figures 4 and 5 show that current I_{4*C1} consists of I_2 en I_3, where I_2 is delivered by the solar cell current I_{sc} and I_3 by capacitor C_a. When the switches 'b' are closed during T_b, the four capacitors C_1 are series circuited and discharged with current I_5 through the battery with voltage V_b, as depicted in Figure 4. Simultaneously, C_a is charged with current I_4 delivered by the solar cell current

I_{sc}, as depicted in Figures 4 and 6. Note that the average charge of capacitor C_a, during a complete period, is 0, and the voltage on the capacitors C_1 after discharging is equal to ¼V_b. Finally, Figure 7 shows the total current through the battery.

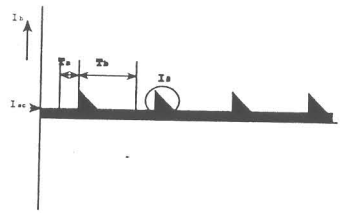

Fig. 7, Battery current.

Current I_{sc} flows during the complete period (T_a+T_b) through the battery and current I_5 during T_b. Below we show that when the voltage over the capacitor C_a, for instance, is equal to the battery voltage, the power delivered to the battery equals the power delivered to the capacitor C_a. Under this condition, half of the solar cell power is delivered directly to the battery at an efficiency of 100%, while the other half is transferred to the battery by means of the switched-capacitor converter.

Note that the currents depicted in Figures 5, 6 and 7 are, in practice, not completely triangularly shaped but for reasons of simplicity the wave-form is simplified to triangle. In the explanation of the parallel power converter it was permissible to assume that they are triangular.

2.1 ANALYSIS OF THE EFFICIENCY

The total efficiency of the parallel power converter is given by

$$\eta_e = \frac{P_{output}}{P_{input}} \tag{2}$$

P_{input} equals

$$P_{input} = (V_b + V_{C_a}) I_{sc} \tag{3}$$

where V_b, V_{ca}, and I_{SC} are the battery voltage, the input capacitor voltage and the solar cell current, respectively. P_{out} can be written as:

$$P_{out} = V_b . I_{sc} + Pconverter.\eta_C \tag{4}$$

where h_C and $P_{converter}$ are the efficiency and the power transported through the switched-capacitor converter, respectively.

Equations 3 and 4 show that, depending on the capacitor voltage and the battery

voltage, a part of the input power is directly delivered to the battery with an efficiency of 100%. $P_{converter}$ can be written as:

$$P_{converter} = P_{input4*C_1} = I_{4*C_1}.V_{C_a} \tag{5}$$

where $P_{input\ 4*C1}$ and V_{ca} are the power delivered to the switched-capacitor converter when the four capacitors C_1 are loaded, and the input capacitor voltage, respectively. Figure 6 shows that the average of I_{4*C1} in one period is equal to I_{sc} and that P_{out} becomes:

$$P_{out} = V_b.I_{sc} + Isubsc.V_{C_a}.\eta_C \tag{6}$$

The efficiency η_C is given by:

$$\eta_C = \frac{P_{output-C}}{P_{input-C}} \tag{7}$$

where $P_{output-C}$ and $P_{input-C}$ are the output power and the input power of the switched-capacitor converter, respectively. $P_{input-C}$ is given by:

$$P_{input-C} = f.I_{4*C_1}.V_{C_a} = \int_{t=0}^{\infty} \left(\frac{V_{C_a} - \frac{1}{4}V_b}{R_S}\right) e^{\left(\frac{-t}{R_S.4C_1}\right)} dt.V_{C_a} \tag{8}$$

where f, I_{4*C1} and R_S are the frequency of the clock signals ϕ_a and ϕ_b, the input current of the switched-capacitor converter and the resistance of the switches, respectively. The solution of Equation 8 is given by:

$$P_{input-C} = f.(V_{Ca} - \frac{1}{4}V_b)4C_1.V_{C_a} \tag{9}$$

which is independent of the switch resistance R_S. With the same method we derive for $P_{output-C}$

$$P_{input-C} = f.(V_{C_a} - \frac{1}{4}V_b)C_1.V_b \tag{10}$$

As a result, the efficiency η_C of the switched-capacitor converter is given by:

$$\eta_C = \frac{P_{output-C}}{P_{input-C}} = \frac{1}{4}\frac{V_b}{V_{C_a}} \tag{11}$$

The total efficiency of the parallel power converter h_e is given by:

$$\eta_e = \frac{V_b . I_{sc} + I_{sc} . \frac{1}{4} V_b}{(V_{C_a} + V_b) . I_{sc}} = \frac{\frac{5}{4} V_b}{V_{C_a} + V_b} \qquad (12)$$

where V_{Ca} has a minimum voltage of ¼V_b, because the voltage on the series connected capacitors C_1 equals ¼V_b after being discharged by the battery.
Before we discuss the results of Equation 12 we give a brief description of a solar cell. Figure 8 shows the substitution diagram with a load R, and Figure 9 shows the I-V and power characteristics of a solar cell.

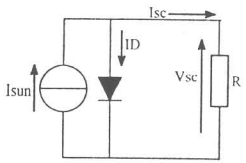

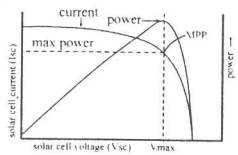

Fig. 8, Substitution diagram of solar cell. Fig.9, Solar cell P-I-V. characteristic.

The solar cell voltage is defined by the load R connected to the output of the solar cell. Figure 9 shows the output current I_{SC} as a function of the output voltage V_{SC} when R varies from 0 to ∞. The maximum output voltage (V_{SC}) of the solar cell is equal to the forward-biased diode voltage. Figure 9 also shows the output power (V_{SC}*I_{SC}) of the solar cell. The maximum is called the Maximum Power Point (MPP).
Figure 10 shows the results of Equations 11 and 12 and the clock frequency of the switched-capacitor converter. It shows the efficiency improvement when parallel power conversion is used instead of a switched-capacitor converter only. Both converters reach their maximum efficiency when V_{Ca} is equal to ¼V_b, but at that point there is no energy transfer to the battery because there is no longer any voltage difference between the series connected capacitors C_1 and the battery. This also becomes clear when we look at the characteristic of the normalized frequency in Figure 10.

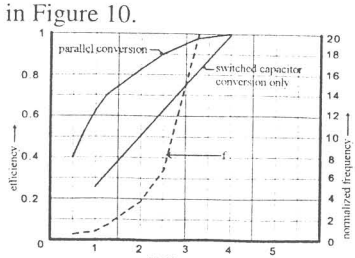

Fig. 10, Efficiency of parallel converter versus SC-converter only.

The theoretical frequency increases rapidly to ∞ when the voltage V_{Ca} becomes equal to ¼V_b. This is obvious when we look at Equations 9 and 10 where we can see that the frequency is inversely proportional to (V_{Ca}-¼V_b).C_1. The frequency in Figure 10 is normalized by making C_1 equal to one.
The Maximum Output Power Point (MOPP) of the parallel power converter is found by multiplying the power characteristic of the solar cell with the results of Equation 12 and reducing this result by subtracting the switching losses.
These losses are caused by the fact that the capacitors in the oscillator and the parasitic capacitors consume considerable power at high frequencies. Simulations have shown that the MOPP is a function of the battery voltage. An overall optimum is reached when the converter operates at the Maximum Power Point (MPP) of the solar cell.

2.2 MAXIMUM-POWER-POINT TRACKER (MPPT)

In the previous Section, we showed that the MPP of the solar cell equals the MOPP of the parallel power converter. In this Section, we present a system[6] that controls the frequency of the parallel power converter to force the solar cell to operate at the MPP.
Because of the nonlinear property of the power characteristic, the controller forces the parallel power converter to track on the MPP of the solar cell by positive feedback of the output current.[6,7] This controller is named Maximum Power-Point Tracker (MPPT). The MPP of the power characteristic is a marginally stable point. The output current, used to track the MPP, is proportional to the input power when the output voltage and
power losses are fairly constant. In the form of an Equation this is:

$$I_{output} \cdot V_b = I_{input} \cdot V_{SC} \tag{13}$$

$$I_{output} = \frac{I_{input} \cdot V_{sc}}{Vsubb} \approx P_{input}(V_b = constant) \tag{14}$$

where V_b and V_{SC} are the battery voltage and the solar cell voltage, respectively. If we wish to use the output current of the parallel power converter, we must multiply this current by a factor that is inversely proportional to the efficiency. The efficiency is a function of the battery voltage and the solar cell voltage. Above, we showed in Equations 11 and 12 how the efficiency depends on those voltages.
For implementation considerations, we used the switched-capacitor output current instead of the total parallel converter output current for maximum power-point tracking. If we wish to use the output current of the switched-

capacitor converter as the control parameter, we must multiply this current by two factors. One factor, as derived, is inversely proportional to the efficiency of the switched-capacitor converter, and the other is inversely proportional to the percentage of input power delivered to the switched-capacitor converter. The efficiency is given by Equation 11 and the percentage of input power is given by $V_{Ca}/(V_b+V_{Ca})x100\%$. The output current must be multiplied by the factor:

$$\frac{V_{Ca}}{4V_b}\cdot\frac{V_b+VsubCa}{V_{Ca}}=\frac{V_b+V_{Ca}}{4V_b}=\frac{V_{SC}}{4V_b} \qquad (15)$$

Because V_b is fairly constant, the switched-capacitor output current need only be multiplied by the solar cell voltage V_{SC}.
Figure 11 shows the control scheme of the MPPT.

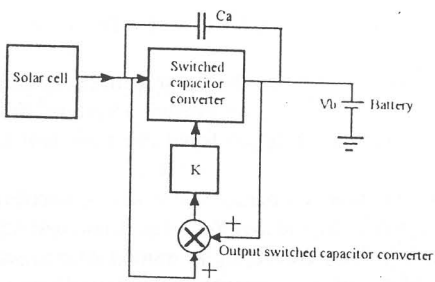

Fig.11, Control scheme.

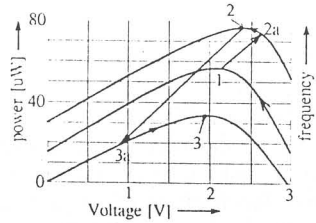

F ig.12, Solar cell P-V characteristics under changing solar insolation.

2.3. MPPT OPERATION

In this section, the MPPT operation is further explained with the aid of Figure 12. Figure 12 shows the P-V characteristics of a solar cell. Points 1 through 3 are the Maximum Power Points of these characteristics. Say that at MPP 1 the light intensity increases. The input voltage and output current increases and, consequently, the frequency of the switched-capacitor converter increases. When point 2a is reached, the input voltage cannot increase further. Then the positive feedback forces the input voltage to point 2, corresponding to the MPP in this situation. When the intensity decreases, the input voltage and the output current decrease, the frequency is also decreasing until point 3a is reached. At point 3a, the input voltage starts to increase, because the switched-capacitor converter input current is smaller than the solar cell current. The output current is then also increasing and by the positive feedback point 3 is reached corresponding to the MPP in this new situation. In practice, there will be a steady-state error[8] depending on the loop gain K. A too large value of K can cause oscillation of the

MPPT loop.

3. SOLAR CELL AREA

In this Section, the derivation of the necessary solar cell area with the aid of data from [9] is discussed. The derivation of the cell area starts with the calculation of the delivered power to a solar cell. This power is delivered by radiation sources such as the sun and or light bulbs. The spectral distribution of a source 's' is characterized by the spectral power density $P_s(\lambda)$. $P_s(\lambda)$ is defined as the power per unit wavelength (W/m). The power P_s delivered to a solar cell through radiation 's' with $P_s(\lambda)$ is defined as:

$$P_s = \int P_s(\lambda) d\lambda [W] \tag{16}$$

The spectral sensitivity of a solar cell is given by:

$$R(\lambda) = R_0 . r(\lambda) \tag{17}$$

where R_0 and $r(\lambda)$ are the maximum sensitivity (A/W) of a solar cell and the relative spectral sensitivity of a solar cell to radiation with wavelength λ, respectively.
The radiation power P_s obtained in Equation 16 generates a current O_{SCs} in the solar cell given by:

$$O_{SCs} = \int R(\lambda) P_s(\lambda) d\lambda = R_0 \int r(\lambda) P_s(\lambda) d\lambda [A] \tag{18}$$

where R_0, $r(\lambda)$ and $P_s(\lambda)$ are the maximum sensitivity of a solar cell, the relative spectral sensitivity of a solar cell to radiation with wavelength λ, and the spectral power distribution of radiation 's'. The detection sensitivity (radiant efficacy) R_{SCs} of the solar cell to radiation 's' is given by:

$$R_{SCs} = \frac{O_{SCs}}{P_s} = R_0 \frac{\int r(\lambda) P_s(\lambda) d\lambda}{\int P_s(\lambda) d\lambda} = R_0 \eta_{SCs} [A/W] \tag{19}$$

where η_{SCs} is the detection efficiency of the solar cell for radiation 's'. η_{SCs} gives the efficiency of detecting radiation 's' compared with the maximum sensitivity R_0.
With the aid of Equation 19, we can start the calculation of the solar cell area. This is done for ambient radiation sources, so the subscript 's' in the previous Equations is replaced by 'a'. The generated electrical power by a solar for

ambient radiation can be calculated by the following Equation

$$P_a = r_a . E_a . A_a \tag{20}$$

where P_a, r_a, E_a and A_a are the generated electrical power, the conversion efficiency of solar cells for ambient light, the irradiance and the solar cell area, respectively. The solar cell must deliver a power P_a of 60 µW with a worst case value E_a of 200 lux .[9] The conversion efficiency r_a is given by:

$$r_a = R_{SCa} . V_{SC} \tag{21}$$

where R_{SCa} and V_{SC} are the radiant efficacy of the solar cell for ambient radiation and the solar cell voltage, respectively. The detection efficiency η_{SCa} of the solar cell for different sources given is by:[9]
solar light $\eta_{SCa}=0.50$
incandescent light of 2856K $\eta_{SCa}=0.27$
incandescent light of 3000K $\eta_{SCa}=0.30$

R_{SCa} for this sources with a maximum sensitivity R_0 of 0.5 A/W is calculated with Equation 19:
solar light $R_{SCa}=0.50*0.5=0.25$ A/W
incandescent light of 2856K $R_{SCa}=0.27*0.5=0.135$ A/W
incandescent light of 3000K $R_{SCa}=0.30*0.5=0.15$ A/W

The conversion efficiency r_a for this sources with an average solar cell voltage of 0.45 V is given by:
solar light $r_a=0.25$ A/W*0.45V =0.11 = 12%
incandescent light of 2856K $r_a=0.135$ A/W*0.45V =0.061 = 6.1%
incandescent light of 3000K $r_a=0.15$ A/W*0.45V=0.068 = 6.8%
The calculation of A_a is not directly possible, because E_a is defined in a photometric unit and R_{SCa} is defined in a radiometric unit. R_{SCa} must be transformed in photometric units for the calculation of A_a. Photometric units are based primarily on the spectral response of an average young human observer. All photometric measurements are weighted by the spectral response of the average eye. The relation between radiometric and photometric units is given by the international standardized eye sensitivity characteristic:

$$V(\lambda) = V_0 v(\lambda) [lm/W] \tag{22}$$

where V_0 and $v(\lambda)$ are the maximum eye sensitivity and the relative eye sensitivity characteristic, respectively. $v(\lambda)$ is at its maximum (1) when V_0 has a wavelength of 555 nm and a sensitivity of 680 lm/W. $V(\lambda)$ introduces the

sensitivity of the eye in lumen for radiation with wavelength λ and a power of 1 Watt.
The luminous efficacy R_{vs} for radiation 's' is defined in the same way as the radiant efficacy R_{SCs}:

$$R_{vs} = V_0 \frac{\int v(\lambda) P_s(\lambda) d\lambda}{\int P_s(\lambda) d\lambda} = V_0 \eta_{vs} [lm/W] \tag{23}$$

where $P_s(\lambda)$ an η_{vs} are the spectral power distribution of radiation 's' and the luminous efficiency, respectively. η_{vs} defines the usefulness of the radiation spectrum as visible light in relation to the maximum eye sensitivity.
With the aid of Equation 23, it is possible to transform conversion efficiency r_a into photometric units. This is done by calculating the luminous efficacy R_{vs} for ambient radiation (R_{va}) for the incandescent light. We are especially interested in incandescent light because the directional hearing aid will, most of the time, operate in this light. The η_{vs} of incandescent light of 2856K and 3000K is 0.03 and 0.044, respectively.[9] R_{va} is then:

incandescent light of 2856K R_{va}=0.03*680lm/W =20.4 lm/W
incandescent light of 3000K R_{va}=0.044*680lm/W =30 lm/W

r_a can be given in photometric units by dividing radiant efficacy R_{SCa} by R_{va} and multiplying this by the solar cell voltage (0.45 V):

incandescent light of 2856K r_a=6.6mA/(lux.m^2)*0.45 V =3.0mW/(lux.m^2)
incandescent light of 3000K r_a=5mA/(lux.m^2)*0.45 V =2.3mW/(lux.m^2)

With r_a in photometric units we can now calculate the solar cell area A_a with Equation 20 and an average r_a of 2.7mW/(lux.m^2) :

$$A_a = \frac{P_a}{E_a . r_a} = \frac{60\mu W}{200lux. \frac{2.7mW}{lux.m^2}} = 1.1 cm^2 \tag{24}$$

4. BLOCK DIAGRAM OF THE POWER CONVERTER

Figure 13 shows the total block diagram of the power converter.

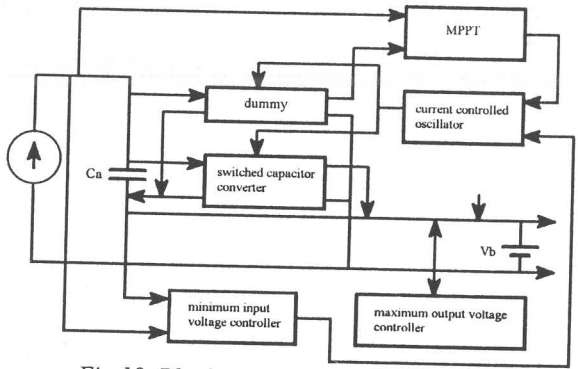

Fig.13, Block diagram of the converter.

The switched capacitor converter is controlled by the oscillator. The input signal of the oscillator is provided by the MPPT through multiplying the solar cell voltage and the dummy output. The dummy is a current sense circuit that measures the output current of the switched-capacitor converter. The circuit of the dummy is identical to the circuit of the switched-capacitor converter, but with smaller capacitors. Because both circuits are identical, the output current of the dummy is proportional to the output current of the switched-capacitor converter. The minimum input voltage controller controls the difference between the input voltage and the output voltage. There is no power transfer from the solar cell to the battery when the difference is equal or smaller than $\frac{1}{4}V_b$, as explained in Section 2.1. At this point, the switching has no longer a function. The oscillator only consumes energy and is switched off through the controller.

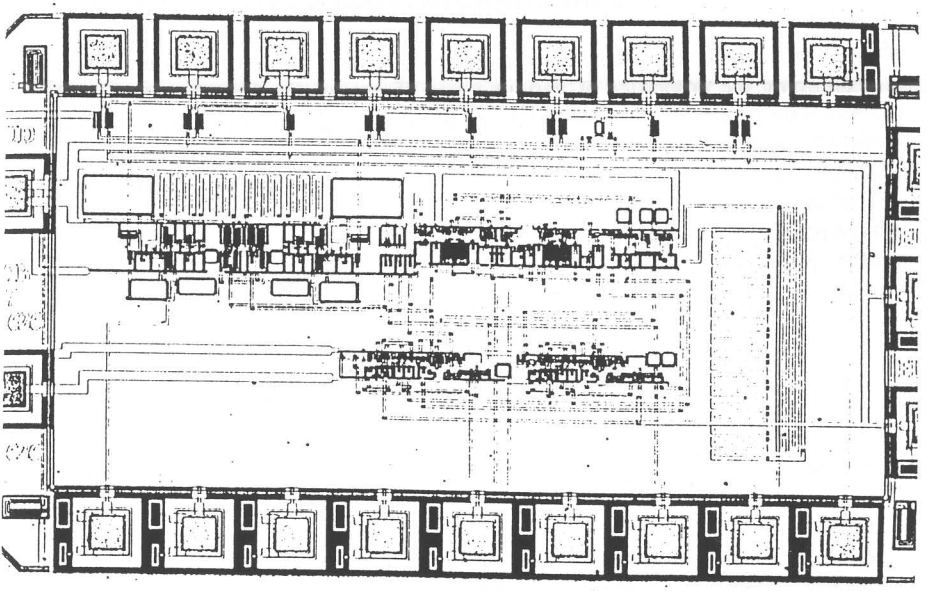

Fig. 14, Photomicrograph of the CMOS chip.

The maximum output voltage controller limits the output voltage to the maximum permissible battery voltage. The battery is a rechargeable thin-film Lithium-ion micro-battery. Under continuous charging, the loading voltage must not exceed the maximum value because the internal impedance will increase and the battery performance deteriorates.

The controller measures the output voltage of the parallel converter and starts to sink the converter output current to ground when this voltage becomes higher than the maximum permissible battery voltage. Consequently, the supply voltage equals the battery voltage during the loading process. One could suggest another control mechanism, where the converter frequency is reduced. However, this is not possible, because the frequency directly controls the current delivered by the switched-capacitor converter, not the current delivered by the capacitor C_a. When the frequency of the switched-capacitor converter is reduced, a increasing part of the solar cell current is delivered to C_a. This causes an increase of the capacitor voltage V_{Ca} , till the maximum solar cell voltage is reached. The increasing capacitor current is passed through the parallel converter output where it causes overcharging of the battery.

The converter has been realized in CMOS on a partial chip. Figure 14 shows a chip photograph. In a later stage, the electronics will be combined with all other electronics needed for the complete system shown in Fig. 1, on one chip.

4.1 THE LITHIUM-ION BATTERY

The decision to implement a rechargeable Lithium-ion battery is taken after examining the properties of various types of potentially feasible batteries. An important property is the possibility of producing this battery with a maximum thickness of 50 µm, which could be directly produced on a substrate. The Department of Chemical Technology and Materials of Delft University of Technology has made a prototype battery of 1.2 V to make practical experiments and measurements possible.
The prototype is made of 4 layers of material, each 35 µm thick and an electrolyte of 60 µm. The battery is symmetrical and looks like this:

$$Metal(Cu)|LiMn_2O_4|BPO_4 - Li|Li_2Mn_2O_4 / LiMn_2O_4|Metal(Cu) \qquad (25)$$

The metal layers function as a current collector and are the battery cathode/anode connections. BPO_4-Li is the electrolyte and is depicted thus because the location of Li is unknown. The electrolyte is, in contrast to most wet electrolytes, that are used, a dry ceramic material, which gives a solid-state battery. The material $LiMn_2O_4$ can cede Lithium-ions in the following way:

$$LiMn_2O_4 \rightarrow Li_{1-x}Mn_2Osub4 + xLi^+ + xe^- \qquad (26)$$

In the layer at the other side of the electrolyte, the following reaction takes place:

$$LiMn_2O_4 + xLi^+ + xe^- \rightarrow x\,Li_2Mn_2O_4 + (1-x)Li\,Mn_2O_4 \qquad (27)$$

The electrons in the previous reactions cause the current in the circuit connected to the battery. The voltage of the battery is fixed by the difference between the redox potentials at both sides of the electrolyte, and is approximately 1.2 V.
Figure 14 shows the charge/discharge voltage characteristic of the prototype. The upper characteristic in Figure 14 is the battery voltage during charging. The lower characteristic is the voltage during discharging. The steps up and down in the voltage at the start and the end of discharging are caused by the internal resistance. The characteristic shows that the battery during discharging does not deliver all the power that is put in during charging. The horizontal axis in this figure gives the charge of the battery divided by the theoretical maximum charge and subtracted from 1. This axis is now equal to the concentration $xLi_2Mn_2O_4$ and (1-x) $LiMn_2O_4$ which disappear during charging. The theoretical maximum capacity is equal to 37.69 mAh, but Figure 14 shows that this prototype is fully

charged when only 5% of this substance is converted. This is can be caused by several factors, like the PVC carrier used to make layers from the substances, the environmental conditions during manufacturing, and the internal resistance.

This prototype has a resistance of 150 Ω in discharged state, and can continuously deliver a current of 10 μA. The high internal resistance is caused by the ceramic electrolyte and the contact between the different layers. The resistance caused by the electrolyte can be reduced by using thinner layers. The contact resistance can be reduced by pressing the layers onto each other with the use of explosives. Research is currently in progress on the construction of better batteries with a reduced internal resistance.

5. SIMULATED RESULTS

As a useful battery is not yet available, the efficiencies of the power converter could not yet be measured. Hence, for the time being, we resort to some simulation results with fixed battery voltages. Figure 15 shows the output power of the solar cell together with the simulated output power characteristics for a

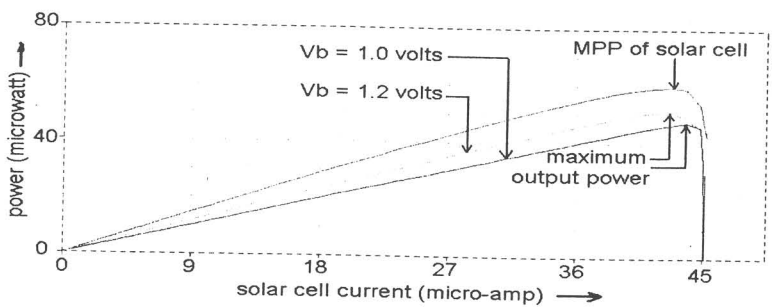

Fig. 15, Simulated power characteristics of the solar cell and converter ou put

fixed battery voltage of 1 and 1.2 Volt, as a function of the solar cell current. The figure shows that the MPP of the solar cell gives a global optimum for the maximum output power of the parallel converter.

6. SMALL TEMPERATURE DIFFERNCES AS ENERGY SOURCES

In this section we introduce the possibility to use small temperature differences feeding a thermo-pile as an electric power supply. Obviously, the amount of energy that can be generated, will be rather small, i.e. maximally a few hundreds of micro-watts. Hence the application area will be restricted to low-power (electronic) systems. Modern thermo-couples, e.g. constructed of the metal

alloys Bismuth/Antimony and Bismuth/Tellurium, provide 354 micro-volts/°C of temperature difference. To keep the thermo-pole reliable as part of an implanted device. the number of seroes-circuited thermo-couples must be restricted. A reasonable value of the feasible output voltage is 5-10 mV. Fig. 16 shows a first experiment of a circuit, that converts the dc output voltage of a thermo-pile, i.e.5-10 mV, to an ac voltage of several volts. After rectifying the resulting dc output voltage is useful for feeding low-power electronics. The operating principle is as follows Normally, a JFET cannot provide voltage gain at drain voltages of a few mV. However, its *current gain* is almost infinite yet. Hence, the *energy gain*, i.e. the product of current gain and voltage gain, easily can exceed the value of one, which is needed to construct an oscillator. In the circuit of Fig.16 the drain voltage is swung up 1500 times, so that it starts oscillating at supply voltages from 4 mV and higher.

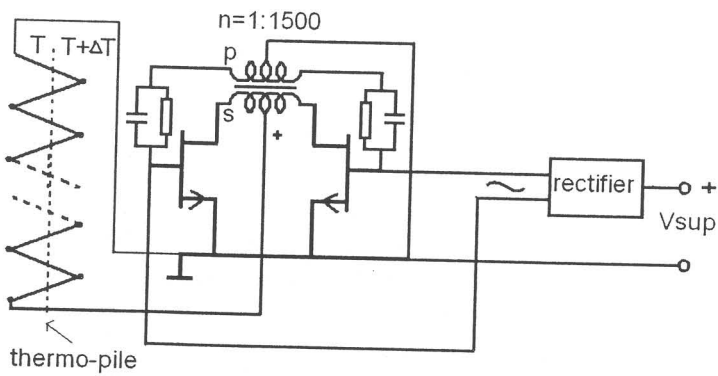

Fig 16, mV- converter, fed by a thermo-pile

7. EM-WAVES AS SUPPLY SOURCES

As the investigations into the usability of wasted EM energy for supplying electronics has very recently started, we only briefly go into it. A feasibility has shown, that e.g. the transmitted energy of a GSM handset is sufficient to provide a quick recharge of the batteries of medical implanted devices, such as pacemakers and neuro-stimulators. In that case these devices have to be redesigned and supplied with rechargeable batteries, such as e.g. Lithium-ion batteries (see section 4-1). A suitable name for this way of energy-gaining could be "ether smog recycling"). An important consequence of the use of wasted EM energy as a supply source is that the (low-power) electronics must be immune to the EM-radiation. To date, a Ph.D. student in our group carries out research into

this subject. Our final goal is to find a couple of design rules for low-power electronics, so that radiated EM waves don't deteriorate the proper functioning of the electronic circuits. Fig.17 shows a possible application, i.e. a quick recharge of a pacemaker's battery by a GSM handset..

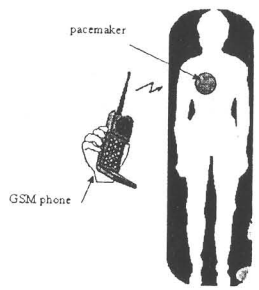

Fig. 17, Quick recharge of a pacemaker's battery by a GSM handset.

8. CONCLUSIONS

The necessary supply power of many electronic systems has decreased such, that the following supply sources are feasible now (or soon):

- Very small solar cells (in progress)
- Small temperature differences (feasibility shown)
- Wasted electromagnetic energy ("ether smog recycling")

9. REFERENCES

1 Dijk, L.P.L. van, Woerd, A.C. van der, and Roermund, A.H.M. van. 'An Ultra Low-Power, Low-Voltage Second-Order All-Pass Filter', to appear in February 1998 in: IEEE J. of Solid-State Circuits.

2 Bais, M. A., 'Feasibility study for the power supply of the directional hearing aid', internal report (in Dutch), Electronics Research Laboratory, Faculty of Electrical Engineering, Delft University of Technology, Delft the Netherlands, November 1996.

3 Bingham, David, 'Locally generated DC power supplies', New Electronics V.20 n.4, pp.18 February 1987.

4 Bates J. B., Gruzalski G. R., Dudney N. J., Luck C. F., Yu X. H., Jones S. D., 'Rechargeable Thin-Film
Lithium Micro-batteries', Solid State Technology, pp. 59-64, July 1993.

5 Snyman D.B., Enslin J.H.R., 'Combined low-cost, High-Efficient inverter, peak power tracker and regulator for pv applications', IEEE Power electronics specialist conference V1, pp.67-74, 1989.

6 Snyman D.B., Enslin J.H.R., 'Simplified feed-forward control of the maximum power point in pv installations', Proceedings of the 4th European Power Electronic Conference, pp. 1265-1270, 1991.

7 Redl and Sokal, 'Near-Optimum Dynamic Regulation of DC-DC Converters Using Feed-Forward of Output Current and Input Voltage with Current-Mode Control', IEEE Transactions on Power Electronics, Vol. PE-1, No. 3, pp. 181-19, 1 July 1986.

8 Slotline and Li, 'Applied Nonlinear Control', Prentice-Hall, 1991.

9 Opto-electronics, System design considerations, GE/RCA publication 1987.